J. Fluid Mech. (1989), *vol.* 208, *pp.* 355–373
Printed in Great Britain

Separation in a gas centrifuge at high feed flow rate

By ZHANG CUNZHEN† AND A. T. CONLISK
Department of Mechanical Engineering, The Ohio State University, Columbus, OH 43210, USA

(Received 28 November 1988 and in revised form 11 April 1989)

The separation of a binary gas mixture for high feed flow rates such that the $E^{\frac{1}{4}}$ vertical shear layer is nonlinear is considered. Numerical solutions for the velocity field and the temperature within the centrifuge are computed using the method originally described by Bennetts & Hocking (1973). These solutions are inputs to the separation problem which is characterized by a concentration boundary layer also of width of $O(E^{\frac{1}{4}})$. Results are presented for a wide range of parameters and the effect of thermal drive strength is examined in detail. Surprisingly the numerical results indicate that the analytical solution for the separation factor given by Conlisk, Foster & Walker (1983) may be used far outside its strict asymptotic region of validity.

1. Introduction

It has been known for many years that gas centrifugation may be employed to separate two-component mixtures. In this problem a two-component gas is fed into a rapidly rotating container and, because of the high rotation speed, the heavier component will be forced to the outer wall and the gas will be enriched in the lighter component near the inner wall (figure 1). In recent years a relatively extensive literature has emerged and, in general, three approaches have been taken to solve the problem. First, both the fluid mechanics and mass transfer have been solved numerically (see for example Kai 1975, 1977); second, the flow field has also been solved by eigenfunction expansion using the so-called 'pancake equation' with the mass transfer problem being solved numerically (Wood & Sanders 1983); and finally, asymptotic analysis has been employed for both the flow and the mass transfer problems leading to closed-form solutions for the velocity field (Conlisk, Foster & Walker 1983; Conlisk 1983; Conlisk 1986*b*) and in a certain parameter range for the mass transfer problem as well. It is this third approach that will be taken in the present work. It should be noted that the problem to be discussed here has a history dating back to World War II and a great body of material had been published prior to the work by Kai (1975). However, much of this early work suffered from the need to make unrealistic assumptions concerning the flow field within the centrifuge. Often the effect of the side- or endwalls was neglected and solutions were produced for vanishingly small feed flow rates. Moreover, radially averaged solutions for the mass fraction of lighter species were often produced which tended to obscure the process of the radial and vertical separation of the mixture taking place (see the reviews by Olander 1981; Soubbaramayer 1979 and Conlisk 1986*b* for discussion of the early work). It has been the goal of this relatively recent work (here defined as that work subsequent to about 1975) to improve understanding of the flow field in

† Permanent address: Department of Engineering Physics, Tsinghua University, Beijing, PRC.

a gas centrifuge and to use the results to obtain better predictions of the separation capacity of a given machine as a function of the operating parameters.

The flow field within a gas centrifuge is complicated and it is perhaps instructive to review the general characteristics of the flow.

The centrifuge considered here is of the Zippe or Groth (Olander 1981; Conlisk 1986*b*) type and is shown in cross-section in figure 1; the arrows denote the qualitative direction of the flow patterns and it is useful to review the structure of the basic source–sink flow patterns. Referring then to figure 1(*a*), the gas enters the container at the feed port (F) through a small slot of width $O(E^{\frac{1}{2}})$ (here E is the Ekman number; $E = \nu/(B_1^2\Omega) \ll 1$ where Ω is the rotation rate, ν the kinematic viscosity, and B_1 the dimensional outer radius) into a vertical Stewartson Layer of width $O(E^{\frac{1}{3}})$; the purpose of this layer is to pass fluid from the feed to the product port (P) at $z^* = L$. Since $E^{\frac{1}{2}} \ll E^{\frac{1}{3}}$ for $E \ll 1$, the product and feed ports are small on the scale of the $E^{\frac{1}{3}}$ layer and appear as point singularities of the $E^{\frac{1}{3}}$-layer equations (Conlisk *et al.* 1983; Conlisk & Walker 1982). Next, the fluid that does not pass out the product port enters a thicker Stewartson layer of width $O(E^{\frac{1}{4}})$; the purpose of the $E^{\frac{1}{4}}$ layer is to adjust the swirl velocity v to relative rest on the sidewall(s) and the vertical velocity is antisymmetric with respect to $z = L/2B_1$ (figure 1). The fluid then passes through the Ekman layers to the outer wall and out of the container (W). For the source–sink component of the motion the only velocity component in the core is an azimuthal swirl. The fraction of fluid that passes out the product port is the cut and is a major parameter in assessing the separation characteristics of the gas centrifuge. Since the Ekman number $E \approx 10^{-7}$–10^{-9} for the centrifuge applications, these boundary layers are extremely thin and in general, comprise less than 5% of the total container volume.

The flow patterns depicted in figure 1 are due to at least three effects; these are (i) an applied temperature gradient, usually vertical (a *thermally driven* centrifuge); (ii) differential rotation of the side- or endwalls which is a model for the scoop drive in a *mechanically driven* centrifuge. Figure 1(*b*) depicts the flow patterns for a thermal or scoop drive which is usually modelled by a differentially rotated end cap. These flow patterns are qualitatively similar to those for source–sink motion and for a parameter $q = \lambda_m(\lambda_1 - \lambda_0) - \frac{1}{2}\lambda_T < 0$ oppose the source–sink motion on $r = a$. Furthermore, locations of thermal or rotational discontinuities act as sources or sinks of fluid as described in Conlisk *et al.* (1983). Theoretically, each of the corners may exhibit a singularity and, for simplicity, only the case where singularities occur in the top corners is depicted in figure 1(*b*). The leading-order (constant) core temperature is T_0^*. (iii) Finally, an imposed source–sink motion is present in all centrifuges. Note that for a purely source–sink flow, there is no *net* motion within the core; moreover, the primary effect of the scoops and/or the small vertical temperature gradient ΔT is to induce a vertical drift within the core region in addition to a swirl component. The presence of this core drift alters the flow patterns in the sidewall boundary layers and, if properly designed, enhances separation significantly (Conlisk 1986*b*).

The purpose of the present paper is to extend the asymptotic results of Conlisk *et al.* (1983) to higher flow rates. This necessitates the consideration of the nonlinear $E^{\frac{1}{4}}$-layer problem and is a significant complication in the mass transfer work.

The plan of this paper is as follows. In §2 the governing equations are presented, and in §3 the nonlinear $E^{\frac{1}{4}}$ layer is considered. In §4 the results of §3 are employed to solve the mass transfer problem. The implications for future work and the conclusions are presented in §5.

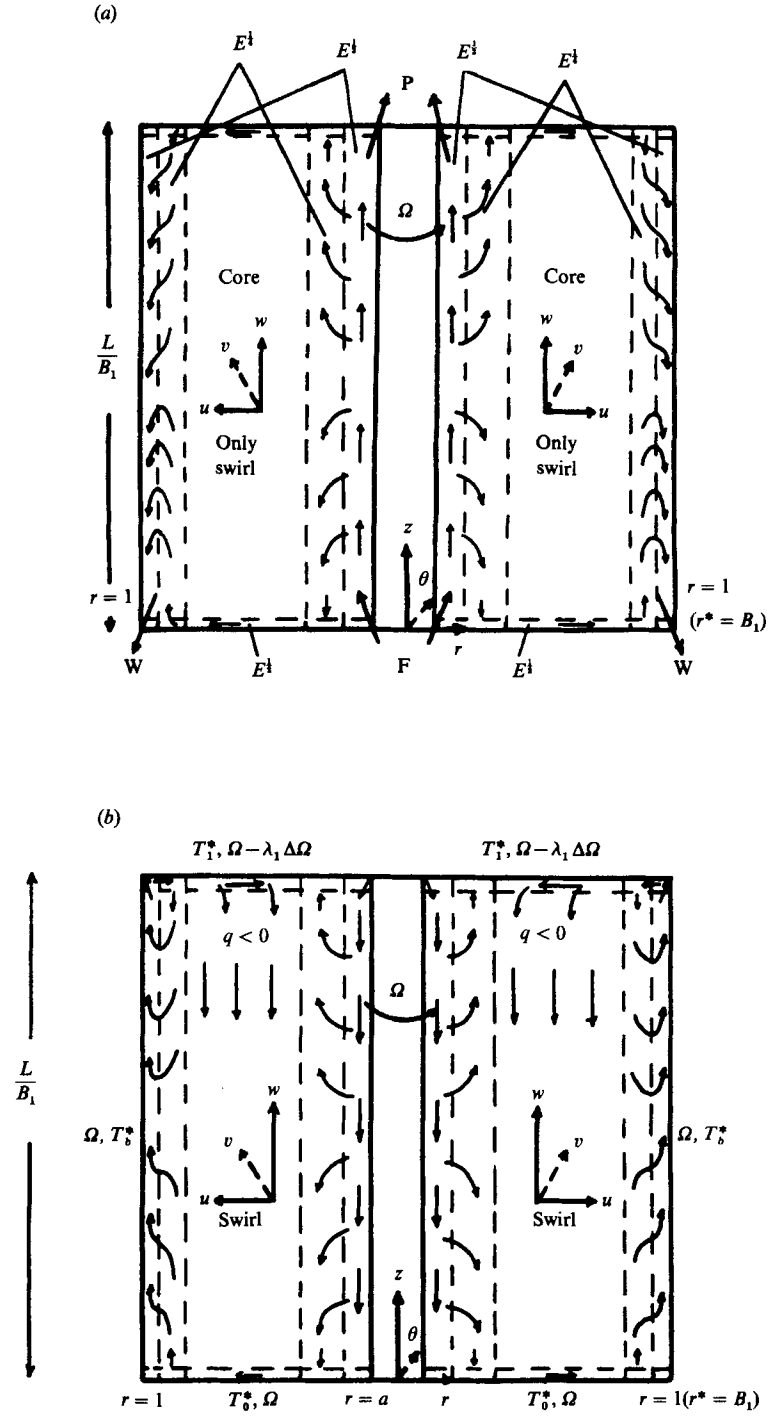

FIGURE 1. Schematic of the Zippe or Groth machine in cross-section; the boundary layers are greatly expanded in scale. (*a*) Qualitative *source–sink* flow patterns. (*b*) Qualitative flow patterns for a positive $\Delta T = T_1^* - T_0^*$ or *scoop* drive modelled by $\lambda_m < 0 (q < 0)$. A special case where $\lambda_0 = 0$ is shown for simplicity. The boundary-layer substructure near the corners of the centrifuge is not shown. See Conlisk *et al.* (1983) for details. This is essentially figure 1 of Conlisk (1986*b*).

2. Governing equations

The basic centrifuge configuration is depicted in figure 1 and consists of an annular region bounded by horizontal end plates at $z^* = 0$ and $z^* = L$. As in Conlisk *et al.* (1983) we write the velocity and temperature fields as perturbations from the basic state of solid-body rotation; non-dimensionalizing all lengths on the outer radius B_1 and velocities on a suitably defined injection velocity U_I. The governing equations are

$$\frac{\partial u}{\partial r}+\frac{u}{r}+\frac{\partial w}{\partial z}+rM^2u=0, \tag{1}$$

$$\epsilon_f\left\{u\frac{\partial u}{\partial r}+w\frac{\partial u}{\partial z}-\frac{v^2}{r}+\rho T\right\}-2v=-rT-\frac{1}{M^2}\frac{\partial p}{\partial r}+\frac{E}{\rho_e(r)}\left\{\nabla^2u-\frac{u}{r^2}-\tfrac{1}{3}M^2\frac{\partial}{\partial r}(ru)\right\}, \tag{2}$$

$$\epsilon_f\left\{u\frac{\partial v}{\partial r}+w\frac{\partial v}{\partial z}+\frac{uv}{r}\right\}+2u=\frac{E}{\rho_e(r)}\left\{\nabla^2v-\frac{v}{r^2}\right\}, \tag{3}$$

$$\epsilon_f\left\{u\frac{\partial w}{\partial r}+w\frac{\partial w}{\partial z}\right\}=-\frac{1}{M^2}\frac{\partial p}{\partial z}+\frac{E}{\rho_e(r)}\left\{\nabla^2w-\tfrac{1}{3}M^2r\frac{\partial u}{\partial z}\right\}, \tag{4}$$

$$\epsilon_f Pr\left\{u\frac{\partial T}{\partial r}+w\frac{\partial T}{\partial z}\right\}-4hru=\frac{E}{\rho_e(r)}\nabla^2T, \tag{5}$$

where

$$E=\frac{\mu}{\rho_0^*\,\Omega B_1^2},\quad \epsilon_f=\frac{U_I}{\Omega B_1},\quad M^2=\frac{\Omega^2B_1^2}{RT_0^*}, \tag{6}$$

and ρ_0^* is the density at the outer sidewall, Ω the rotation rate, μ the viscosity, R the gas constant, T_0^* the leading-order (constant) temperature in the rotor; U_I is the injection velocity which is defined as

$$U_I=\frac{\dot m_F E^{-\frac{1}{2}}}{\rho_0^*B_1^2} \tag{7}$$

where $\dot m_F$ is the feed dimensional flow rate. The dimensionless perturbation quantities p, ρ and T are defined by

$$p^*=p_e^*(1+\epsilon_f p),\quad \rho^*=\rho_e^*(1+\epsilon_f\rho),\quad T^*=T_0^*(1+\epsilon_f T), \tag{8}$$

where an asterisk denotes a dimensional quantity. Also in (1)–(5)

$$h=\frac{\gamma-1}{4\gamma}PrM^2,\quad \nabla^2=\frac{1}{r}\frac{\partial}{\partial r}\left(r\frac{\partial}{\partial r}\right)+\frac{\partial^2}{\partial z^2},$$

where γ is the ratio of specific heats.

As is usual in the present problem, a perfect gas is assumed, which leads to

$$\rho_e(r)=\exp\left(\tfrac{1}{2}M^2(r^2-1)\right) \tag{9}$$

and

$$p=\rho+T. \tag{10}$$

The governing equation for the separation of a binary mixture in a rapidly rotating flow may be derived using standard arguments (Conlisk *et al.* 1983; Bird, Stewart & Lightfoot 1960) for the case of steady flow and no chemical reactions within the centrifuge; this equation in dimensionless form is given by

$$\rho_e(r)E^{-\frac{1}{2}}(\boldsymbol{Q}\cdot\boldsymbol{\nabla})\omega_A-\delta\epsilon M^2H(\omega_A)=\delta\nabla^2\omega_A, \tag{11}$$

for $a = A_1/B_1 \leqslant r \leqslant 1$ and $0 \leqslant z \leqslant L/B_1 = Z_0$, where

$$H(\omega_A) = 2\omega_A(1-\omega_A)+r\frac{\partial}{\partial r}(\omega_A(1-\omega_A)). \tag{12}$$

In (11) ω_A is the mass fraction of the lighter component of the binary mixture and $\boldsymbol{Q} = (u, v, w)$ is the dimensionless velocity vector in cylindrical components as depicted on figure 1; in (11) the dimensionless parameters δ and ϵ are defined by

$$\epsilon = \frac{M_B - M_A}{M_A}, \quad \delta = \frac{E^{\frac{1}{4}}}{Sc\epsilon_f}, \tag{13}$$

and in (13) M_B and M_A are the molecular weights of the heavy and light species respectively, and Sc is the Schmidt number and is defined by

$$Sc = \mu/\rho^* D_{AB}, \tag{14}$$

where D_{AB} is the diffusion coefficient.

The boundary conditions associated with (1)–(5) are for the velocity field $u = v = w = 0$ on all solid walls, except at points of injection and withdrawal of gas. For the temperature field, there are a number of possibilities. We consider the case where the side- and endwalls are held at constant but differing temperatures. Defining a thermal Rossby number by

$$\epsilon_T = \frac{T_1^* - T_0^*}{T_0^*}$$

we assume that

$$\left.\begin{aligned} T = 0 \quad \text{at} \quad z = 0, \quad T = \lambda_T \quad \text{at} \quad z = Z_0, \\ T = \lambda_a \lambda_T \quad \text{at} \quad r = a, \quad T = \lambda_b \lambda_T \quad \text{at} \quad r = 1, \end{aligned}\right\} \tag{15}$$

where

$$\lambda_a = \frac{T_a^* - T_0^*}{T_1^* - T_0^*}, \quad \lambda_T = \epsilon_T/\epsilon_f,$$

and T_a^*, T_1^* and T_0^* are the temperatures at $r = a$, $z = Z_0$ and $z = 0$, respectively, and all are constant. The definition of λ_b is analogous.

The case of differential rotation is analogous and may be considered in a similar way; in this paper, however, we consider only the case of thermally driven flow.

A major limitation of the mass transfer work presented in Conlisk *et al.* (1983) is that the boundary conditions associated with (11) are valid only for $\delta \gg E^{\frac{1}{4}}$. However, flow rates of practical interest are nominally within the regime $\delta \gtrsim E^{\frac{1}{4}}$ and so it is important that the mass transfer problem be considered for $\delta = O(E^{\frac{1}{4}})$. The complicating feature of this parameter range is that, for $Sc = O(1)$, $\epsilon_f = O(E^{\frac{1}{4}})$ (from (13)) and it is in this regime that the $E^{\frac{1}{4}}$ layer becomes nonlinear. Before reconsidering the sidewall boundary condition for (11) in §3 the nonlinear compressible $E^{\frac{1}{4}}$ layer is analysed.

3. The compressible nonlinear $E^{\frac{1}{4}}$ layer

3.1. *Governing equations*

It is well known that as the Rossby number ϵ_f increases, the nonlinear terms in (2)–(4) first become important in the $E^{\frac{1}{4}}$ layer (Bennetts & Hocking 1973); furthermore, the $E^{\frac{1}{4}} \times E^{\frac{1}{4}}$-layer section underneath the $E^{\frac{1}{4}}$ layer (Conlisk *et al.* 1983) becomes nonlinear at the same time so that the linear Ekman condition cannot be used as was done in Barcilon (1970). Consequently, the problem is significantly more complicated than in

the linear case. It should be noted that the solution in all the other regions of the flow remain the same as in Conlisk *et al.* (1983). In what follows let $\epsilon_t = \lambda E^{\frac{1}{4}}$.

In the $E^{\frac{1}{4}}$ layer on $r = a$ let $\xi = (r-a)E^{-\frac{1}{4}}$ and expand the velocities, temperature and pressure as

$$\left.\begin{aligned} u = E^{\frac{1}{2}}u_0+\ldots, \quad v = V_G(a)+v_0+\ldots, \quad w = E^{\frac{1}{4}}w_0+\ldots, \\ T = \lambda_a\lambda_T+\hat{T}_0+\ldots, \quad p = E^{\frac{1}{4}}M^2p_0+\ldots, \end{aligned}\right\} \tag{16}$$

where $V_G(a)$ is the swirl velocity in the geostrophic core (see below, (32)). then to leading order, (1)–(5) become

$$\frac{\partial u_0}{\partial \xi}+\frac{\partial w_0}{\partial z} = 0, \tag{17}$$

$$-2v_0+a\hat{T}_0+\frac{\partial p_0}{\partial \xi} = 0, \tag{18}$$

$$\lambda\left(u_0\frac{\partial v_0}{\partial \xi}+w_0\frac{\partial v_0}{\partial z}\right)+2u_0 = \frac{1}{\rho_e(a)}\frac{\partial^2 v_0}{\partial \xi^2}, \tag{19}$$

$$\frac{\partial p_0}{\partial z} = 0, \tag{20}$$

$$\lambda Pr\left(u_0\frac{\partial \hat{T}_0}{\partial \xi}+w_0\frac{\partial \hat{T}_0}{\partial z}\right)-4hau_0 = \frac{1}{\rho_e(a)}\frac{\partial \hat{T}_0}{\partial \xi^2}. \tag{21}$$

It should be noted here that the Mach number is assumed to be $O(1)$. Equations (18)–(21) are extremely complicated because of the coupling of the temperature field and the velocity field.

3.2. *The nonlinear Ekman condition*

As mentioned previously, the $E^{\frac{1}{4}} \times E^{\frac{1}{2}}$ corner region underneath the $E^{\frac{1}{4}}$ layer becomes nonlinear at the same time as the $E^{\frac{1}{4}}$ layer and it seems necessary to calculate a full numerical solution in that region. As Bennetts & Hocking (1973) point out, however, in such an approach, the dependence of the solution on the individual parameters would not be easy to deduce, thereby making it difficult to incorporate the result into a single boundary condition on the $E^{\frac{1}{4}}$-layer solution. In the interest of preserving the structure of the nonlinear $E^{\frac{1}{4}}$ layer, Bennetts & Hocking (1973) derived a nonlinear Ekman condition based on the assumption that the Ekman layer underneath the $E^{\frac{1}{4}}$ layer has a local similarity form. While it is difficult to assess quantitatively the validity of such a procedure, comparison of their results with the experimental results of Hide (1968) reveals general agreement in the thickness of the source and sink layers; moreover, for the Rossby numbers of interest here, the agreement between the experimental results of Hide (1968) and the numerical results of Bennetts & Hocking (1973) is quantitatively good and because of this, the Bennetts & Hocking approach has been adopted here. In the present case of compressible flow, we find that equations (3.2) and (3.3) of Bennetts & Hocking re-emerge with the definitions (in their notation)

$$u_0 = \frac{\partial \psi}{\partial \zeta}, \quad \bar{\chi} = v_0-\tfrac{1}{2}a\hat{T}_0, \quad w_0 = -\frac{\partial \psi}{\partial \xi'}, \tag{22}$$

where $\xi' = (2/\lambda)\xi$, and $\zeta = zE^{-\frac{1}{4}}$, provided $ha^2 \ll 1$ and $Pr \approx 1$. For the case of UF_6 at $T_0^* = 320$ K, the Prandtl number $Pr = 0.95$ and for typical values of the

parameters, say, $M = 3, h = 0.05$; consequently, the Ekman condition that thus emerges is (since $\hat{T}_0 =$ Constant at $z = 0, Z_0$)

$$w_0 = \pm C_E \frac{\partial v_0}{\partial \xi}, \quad z = \frac{0}{Z_0}. \tag{23}$$

Bennetts & Hocking's result for the incompressible nonlinear Ekman condition thus corresponds to the leading-order term in an asymptotic expansion about $h = 0$ and $Pr = 1$. Here $C_E = C_E(\lambda, (\partial v/\partial \xi)|_{\xi=0})$ is a coefficient that is independent of ξ and $0.3 \leqslant C_E \leqslant 0.7$; the linear problem corresponds to $C_E = \frac{1}{2}$. Bennetts & Hocking have given the numerical solutions of C_E for different λ and $(\partial v_0/\partial \xi)|_{\xi=0}$. The values of C_E are in table 1 of their paper (1973). For convenience in the numerical solution we have fitted the Bennetts & Hocking data to specific functional forms. These results are given by

$$C_E = 0.3455 \exp(-0.5050x) + 0.1545, \quad -1 \leqslant x \leqslant 1 \tag{24}$$

and

$$C_E = 0.3630 \exp(-0.3316(x-1)^{0.5970}), \quad 1 \leqslant x \leqslant 10, \tag{25}$$

where

$$x = \tfrac{1}{2}\lambda \frac{\partial v}{\partial \xi}\bigg|_{\xi=0}. \tag{26}$$

Note that for $x = 0$ (i.e. $\lambda = 0$) $C_E = 0.5$ which corresponds to the linear solution. Equations (24) and (25) are then used in the numerical solution as described in the next section.

3.3. *Solution of the nonlinear $E^{\frac{1}{4}}$-layer equation*

Because the sidewall temperatures are assumed to be constant, the swirl and radial velocities and temperature are independent of the variable z and we write the velocities as

$$v_0 = \phi(\xi), \tag{27a}$$

$$u_0 = 2C_E \frac{\sigma^{\frac{1}{4}}(a)}{\rho_e^{\frac{1}{2}}(a)} \phi(\xi), \tag{27b}$$

$$w_0 = -C_E \frac{\sigma^{\frac{1}{4}}(a)}{\rho_e^{\frac{1}{2}}} (z - \tfrac{1}{2}Z_0) \frac{\mathrm{d}\phi}{\mathrm{d}\xi}, \tag{27c}$$

where (27*b*, *c*) are obtained from (17) and (23). Substituting these expressions into (19) yields

$$\frac{\mathrm{d}^2\phi}{\mathrm{d}\xi^2} - 2\lambda C_E \sigma^{\frac{1}{4}}(a) \rho_e^{\frac{1}{2}}(a) \phi \frac{\mathrm{d}\phi}{\mathrm{d}\xi} - 4C_E \sigma^{\frac{1}{4}}(a) \rho_e^{\frac{1}{2}}(a) \phi = 0, \tag{28}$$

subject to

$$\left.\begin{aligned} \phi &= -V_G(a), \xi = 0, \\ \phi &\to 0, \qquad \xi \to \infty. \end{aligned}\right\} \tag{29}$$

Note that (28) is independent of temperature and consequently may be solved in a straightforward manner using finite differences.

The equation for the temperature variation within the $E^{\frac{1}{4}}$ layer may be obtained by substituting (16) into (21) and noting from (18) that $\partial \hat{T}_0/\partial z = 0$. The result is

$$\frac{\mathrm{d}^2\hat{T}_0}{\mathrm{d}\xi^2} - 2\lambda Pr\, C_E \sigma^{\frac{1}{4}}(a) \rho_e^{\frac{1}{2}}(a) \frac{\mathrm{d}\hat{T}_0}{\mathrm{d}\xi} + 8ha\sigma^{\frac{1}{4}}(a) \rho^{\frac{1}{2}}(a) \phi = 0, \tag{30}$$

subject to

$$\hat{T}_0 = 0 \quad \text{at} \quad \xi = 0 \quad \text{and as} \quad \xi \to \infty. \tag{31}$$

Dimensional parameters	Value
B_1	0.25 m
L	2.50 m
ΩB_1	260 m/s
T_0	320 K
$\dot{m}_F$	10^{-4}–10^{-5} kg/s
Dimensionless parameters	**Value**
a	0.3–0.8
M	3
θ	0.2–0.9
q	−10–0

TABLE 1. Range of parameters discussed in the present problem

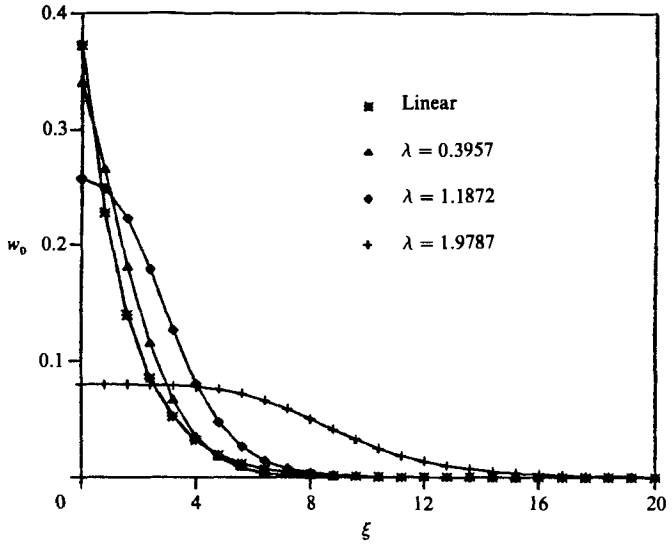

FIGURE 2. Vertical velocity profiles as a function of ξ for $q = -3$ for several values of λ; the profiles are depicted at $z = Z_0$.

It is not obvious that $\hat{T}_0 \to 0$ as $\xi \to \infty$ because the geostrophic problem has not been considered here; (31) is, however, correct as shown in Appendix A. Note that (30) is coupled to the fluid equation (28) and once (28) is solved, then (30) may be solved directly. The methods employed to solve these two equations are discussed in Appendix B.

It should be noted here that the form of geostrophic velocity remains the same as in Conlisk *et al.* (1983) and the result is

$$V_G(a) = \frac{1}{\sigma(a)}\left\{aq(\lambda_a - \tfrac{1}{2}) + \frac{\sigma^{\frac{3}{4}}(a)}{\rho_e^{\frac{1}{8}}(a)}\right\}, \tag{32}$$

where

$$q = -\tfrac{1}{2}\lambda_T \tag{33}$$

for a thermally driven centrifuge (see Conlisk *et al.* 1983).

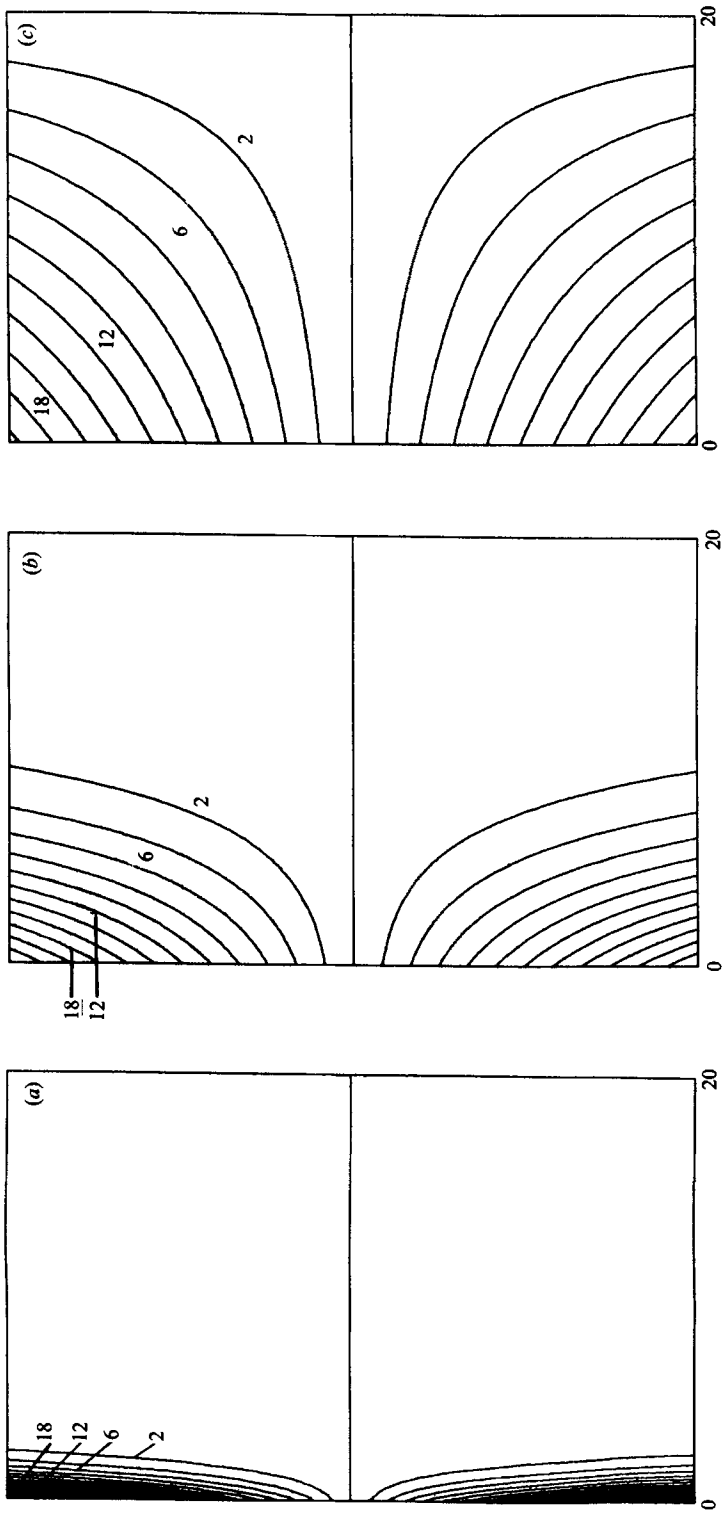

FIGURE 3. Streamline patterns for $q = -3$ for various values of λ. Here the streamline increment is $\Delta\psi = 2$. (*a*) $\lambda = 0.3957$, (*b*) $\lambda = 1.1872$, (*c*) $\lambda = 1.9787$. Note the thickening of the layer as λ increases. The far right boundary of the figure corresponds to $\xi_\infty = 20$.

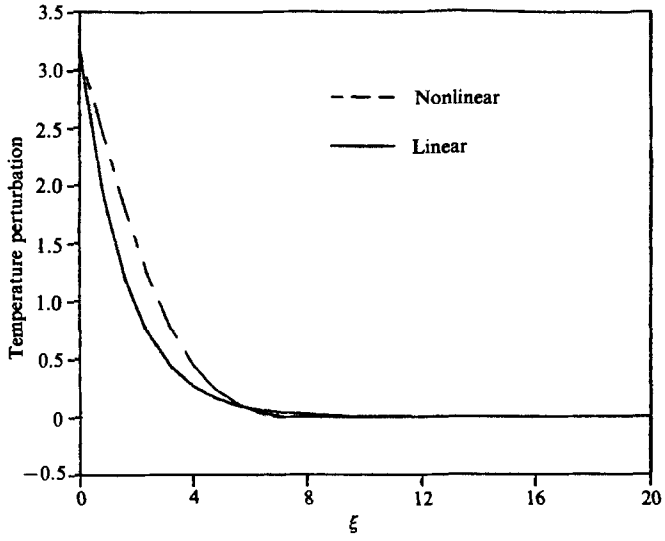

FIGURE 4. Temperature perturbation as a function of ξ for $\lambda = 1.9787$ compared with the linear result, $q = -3$.

3.4. *Results*

To observe the effect of the increased flow rate on the velocity profile in the source layer on $r = a$, numerical solutions have been computed for centrifuge parameters used in Conlisk (1986*b*), and detailed in table 1. Figure 2 shows the solutions for $q = -3$ for several values of λ for the vertical velocity as a function of ξ at the top of the can, $z = Z_0^-$. The values of λ are 0.3957, 1.1872 and 1.9787, respectively, corresponding to the feed mass flow rates $\dot{m}_F = 1 \times 10^{-4}$ kg/s, 3×10^{-4} kg/s, and 5×10^{-4} kg/s. Note that the solution is fairly close to the linear solution for $\lambda = 0.3957$, while the difference for $\lambda = 1.1872$ and 1.9787 is substantially greater.

The streamlines for these cases are shown on figure 3. The stream function ψ is defined in the usual way and is given by

$$\psi = \frac{2\sigma^{\frac{1}{4}}(a)}{\rho_e^{\frac{1}{2}}(a)} C_E \phi(\xi)(z - \tfrac{1}{2}Z_0). \tag{34}$$

On figure 3 (*a–c*) are the solutions for $\lambda = 0.3957$, 1.1872 and 1.9787, respectively, and $q = -3$. Note the significant increase in the width of the $E^{\frac{1}{4}}$ layer as λ increases. Figure 4 illustrates the nonlinear effect on the temperature perturbation for $\lambda = 1.9787$. The results presented in this section are for $\lambda_a = 1$ so that the side- and top endwall are at the same temperature. Other results for different values of $\lambda_a, 0 \leqslant \lambda_a \leqslant 1$ show only a very weak dependence on λ_a and are not reproduced here.

4. The mass transfer equation

4.1. *Basic concentration-layer structure*

The structure of the mass transfer problem for $\epsilon_t \ll E^{\frac{1}{4}}$ which has been treated previously (Conlisk *et al.* 1983; Conlisk 1983, 1986*b*) for small δ consists of a pair of concentration layers of width $O(\delta^{\frac{1}{3}})$ on the vertical surfaces with a single layer of

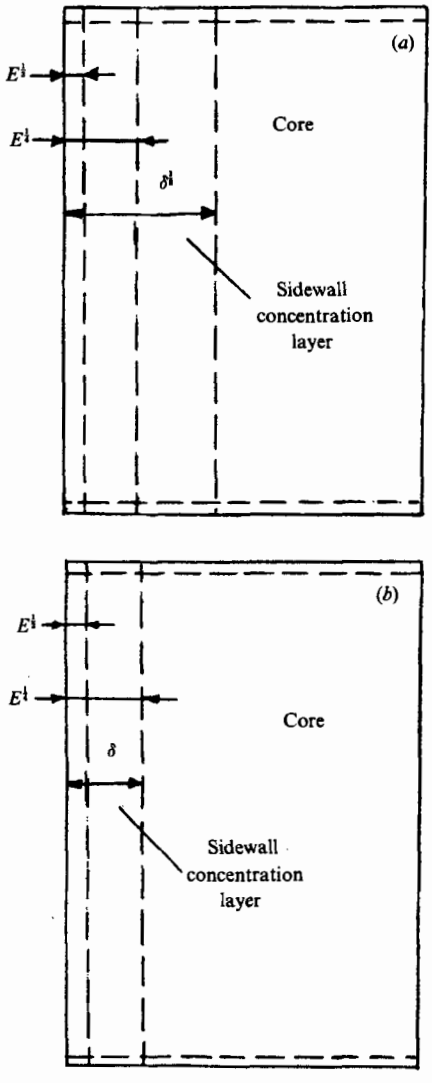

FIGURE 5. (*a*) Sketch of the concentration-layer structure for $\delta \gg E^{\frac{1}{4}}$. (*b*) Sketch of the present concentration-layer structure $\delta = O(E^{\frac{1}{4}})$. Only the vertical shear layer structure is shown.

width $O(\delta)$ on either the top or bottom wall depending on whether the parameter q is greater than or less than zero. These concentration layers surround a core region in which mass diffusion is negligible to leading order. This structure obtains provided $E^{\frac{1}{4}} \ll \delta \ll 1$, and a sketch of this situation is given in figure 5(*a*).

Since $\delta = E^{\frac{1}{2}}/Sc\epsilon_f$, for $\epsilon_f = O(E^{\frac{1}{4}})$ with $Sc = O(1)$, then $\delta = O(E^{\frac{1}{4}})$ and this structure is altered; in this case the width of the mass transfer (or concentration) layer is of $O(\delta) = O(E^{\frac{1}{4}})$, the same width as the outer Stewartson layer as is depicted in figure 5(*b*).

In the present parameter range, the core region of the centrifuge is unaffected by the increase in mass flow rate, with (11) reducing to a balance between pressure diffusion and convection; i.e. for

$$\omega_A = \omega_F + \delta\epsilon M^2 \omega_F (1-\omega_F)\, \omega_1(r,z) \tag{35}$$

then the diffusion terms in (11) are $O(\delta\epsilon M^2)$ and consequently

$$\rho_e W_G \frac{\partial \omega_1}{\partial z} = 2, \tag{36}$$

which is the same equation as considered by Conlisk *et al.* (1983). For $W_G < 0$ (a downward core drift) the solution is given by

$$\omega_1 = C + \frac{2}{\rho_e W_G}(z - Z_0), \tag{37}$$

where C is a constant to be determined. This core distribution is altered as we approach the side- and endwalls and these regions are considered next.

4.2. *The sidewall concentration layer*

In the $E^{\frac{1}{4}}$ layer $w \sim O(E^{\frac{1}{4}})$ and if $\delta = O(E^{\frac{1}{4}})$ convection and diffusion of mass in (11) balance if the width of the concentration layer is the same as that of the fluid layer, i.e. of $O(E^{\frac{1}{4}})$. Thus for $\delta = \beta E^{\frac{1}{4}}, \beta = O(1)$

$$\frac{\partial^2 \tilde{\omega}_1}{\partial \xi^2} = \frac{\rho_e}{\beta}\left(u_0 \frac{\partial \tilde{\omega}_1}{\partial \xi} + w_0 \frac{\partial \tilde{\omega}_1}{\partial z}\right), \tag{38}$$

where u_0 and w_0 are defined in (27) and

$$\omega_A = \omega_F + \delta\epsilon M^2 \omega_F (1 - \omega_F)\, \tilde{\omega}_1. \tag{39}$$

Note that radial convection of mass is now as important as vertical convection and (38) is thus more difficult to solve than in Conlisk *et al.* (1983). Since u_0 and w_0 are both numerical functions, numerical solutions to (38) must be sought.

Equation (38) is subject to boundary conditions at $\xi = 0$ and as $\xi \to \infty$. To deduce the appropriate boundary conditions at the sidewall, we note that the $E^{\frac{1}{3}}$-layer solution for the mass fraction is unaltered from that of Conlisk *et al.* (1983) and is given by

$$\omega_{A\frac{1}{3}} = A_0(z) + \frac{E^{\frac{1}{3}}}{\delta}\bar{\omega}_1(\eta, z), \tag{40}$$

where $\eta = (r - a)\, E^{-\frac{1}{3}}$ and

$$\bar{\omega}_1 = B_0(z) - \rho_e A_0' \int_0^\eta (\eta - t)\, w_2(t, z)\, \mathrm{d}t - \delta\epsilon M^2 a A_0 (1 - A_0)\, \eta; \tag{41}$$

note that the expansion above for the total mass fraction in the $E^{\frac{1}{3}}$ layer, $\omega_{A\frac{1}{3}}$, is slightly different from that in Conlisk *et al.* (1983) in that some scale factors have been removed for clarity. Writing (41) in the $E^{\frac{1}{4}}$-layer variables (i.e. as $\eta \to \infty$) and using the expansion for $\omega_{A\frac{1}{3}}$ above we must have

$$\lim_{\xi \to 0} \omega_A = A_0(z)$$

and

$$\left.\frac{\partial \omega_A}{\partial \xi}\right|_{\xi=0} = \frac{E^{\frac{1}{4}}}{\delta}\left\{\rho_e \left(\int_0^\infty w_2\, \mathrm{d}t\right)\frac{\partial \omega_A}{\partial z} - \delta\epsilon M^2 a \omega_A (1 - \omega_A)\right\}, \quad \xi = 0 \tag{42}$$

from Taylor series considerations. In terms of $\tilde{\omega}_1$ defined in (39), equation (42) is

$$\frac{\partial \tilde{\omega}_1}{\partial \xi} = \frac{1}{\beta}\left(\rho_e F_{\frac{1}{3}} \frac{\partial \tilde{\omega}_1}{\partial z} - a\right) \quad \text{at} \quad \xi = 0. \tag{43}$$

Note that (43) is similar in form to that for $\delta \gg E^{\frac{1}{4}}$, except that $F_{\frac{1}{3}}$ replaces the total shear layer flux $F_{\frac{1}{3}}+F_{\frac{1}{4}}$.

The solution in the layer on $r = b$ is similar except that a minus sign appears before $\partial\tilde{\omega}_1/\partial z$. $F_{\frac{1}{3}}(a)$ is the volume flux within the $E^{\frac{1}{3}}$ layer and is the same as in Conlisk *et al.* (1983).

The problem which must be solved is thus given by (38) subject to (43) and the matching condition as $\xi \to \infty$ which is

$$\tilde{\omega}_1 = C + 2/\rho_e W_G(z - Z_0). \tag{44}$$

However, C is an unknown constant and is obtained by matching to the corner regions. This matching and the numerical solution of this problem are considered next.

4.3. *Solution for the sidewall concentration layer*

To solve (38), the value of $\tilde{\omega}_1$ as $\xi \to \infty$ was subtracted out and the solution for the resulting perturbation was obtained using a marching technique. The scheme proceeds from the top wall down; the standard Crank–Nicholson technique was employed in the z-direction. At each z-location, the Thomas algorithm was used to solve the set of equations that arises from discretizing the radial derivatives. Because of the presence of the convective terms in (38) standard marching procedures will fail if the velocity in the marching direction becomes negative. Thus if $z^* = Z_0 - z$, then for $z < \frac{1}{2}Z_0$ we write

$$\frac{\partial\tilde{\omega}_1}{\partial z^*} \approx \frac{1}{k}(\tilde{\omega}_{1i}^{j+1} - \tilde{\omega}_{1i}^{j}),$$

and for $z^* > \frac{1}{2}Z_0$

$$\frac{\partial\tilde{\omega}_1}{\partial z^*} \approx \frac{1}{k}(\tilde{\omega}_{1i}^{j} - \tilde{\omega}_{1i}^{j-1}),$$

where i denotes the radial location and j the axial location, and k is the z-grid size. Use of this upwind discretization scheme ensured stability of the numerical scheme.

The constant C is obtained by matching to the corner regions at $z = 0$; the procedure is not altered from that described by Conlisk *et al.* (1983) because the extension of the $O(\delta)$ layer under the $E^{\frac{1}{4}}$ layer on $z = 0$ is now of $O(E^{\frac{1}{4}} \times E^{\frac{1}{4}})$ over which (it may be shown) the mass fraction is constant. To describe the matching, let

$$\omega_1^* = \tilde{\omega}_1 - \left\{C + \frac{2}{\rho_e W_G}(z - Z_0)\right\}. \tag{45}$$

In the corner regions at the feed point ($r = a, z = 0$) and waste point ($r = b, z = 0$) the solution $\tilde{\omega}_1$ must match to the solution of the horizontal mass fraction boundary layer, which is given by equation (3.70) of Conlisk *et al.* (1983) (with suitable changes in notation). Taking the appropriate limits of that equation as the radial variable approaches the feed and the waste, we obtain

$$C + \frac{D + a^2}{a\rho_e(a)\, F_{\frac{1}{2}}(a, 0)} = 0 \quad \text{at the feed point,} \tag{46}$$

and

$$C + \frac{D + b^2}{b\rho_e(b)\, F_{\frac{1}{2}}(b, 0)} = \tilde{\omega}_{1W} \quad \text{at the waste point.} \tag{47}$$

The conservation of the light component species gives

$$\tilde{\omega}_{1W} = -\frac{\theta}{1 - \theta}\tilde{\omega}_{1P}. \tag{48}$$

ξ_∞	N	$\Delta\xi$	N_z	Δz	ω_P	α_W	δU (kg U/yr)
10	26	0.40	41	0.25	0.0071362	1.09066	2.3311
14.8	38	0.40	41	0.25	0.0071350	1.08935	2.2538
20	51	0.40	41	0.25	0.0071344	1.08914	2.2207
30	76	0.40	41	0.25	0.0071341	1.08903	2.1925
20	51	0.40	21	0.50	0.0071340	1.08832	2.1756
20	51	0.40	41	0.25	0.0071344	1.08914	2.2207
20	51	0.40	81	0.125	0.0071347	1.08928	2.2418
20	26	0.80	41	0.25	0.0071342	1.08903	2.2147
20	51	0.40	41	0.25	0.0071344	1.08914	2.2207
20	101	0.20	41	0.25	0.0071344	1.08914	2.2207

TABLE 2. Numerical results for the indicated parameters as a function of mesh size. N_z is the number of grid points in the z-direction.

Here $F_{\frac{1}{2}}$ is the volume flow rate in the Ekman layer and θ is the cut. From (45)–(48) the constant C can be determined by

$$C\left(1+\frac{\theta}{1-\theta}-\frac{a}{b}\frac{\rho_e(a)}{\rho_e(b)}\frac{F_{\frac{1}{2}}(a,0)}{F_{\frac{1}{2}}(b,0)}\right)=\frac{a^2-b^2}{b\rho_e(b)F_{\frac{1}{2}}(b,0)}-\frac{\theta}{1-\theta}\omega_{1P}^*, \tag{49}$$

where ω_{1P}^* is the numerical solution of ω_1^* at the product point. The initial guess for C is taken to be zero and successive iteration on the constant C is performed. In the calculations which have been performed, the scheme converged in less than ten iterations with a relative error of less than 10^{-3}.

For the numerical solution typically 51 points were used in the radial direction with 41 points being employed in the axial direction. In table 2 are presented some typical numerical results as a function of grid size. In following calculations we let $\xi = 20$ and grid size $\Delta\xi = 0.40, k = 0.25$.

In what follows, the results for both the separation factor and separative power will be presented for various values of the parameters. Consistent with much of the work in this area we define the total separation factor

$$\alpha_W = \frac{\omega_P(1-\omega_W)}{\omega_W(1-\omega_P)} \tag{50}$$

and the separative power

$$\delta U = \tfrac{1}{2}\dot{m}_F\theta(1-\theta)(\alpha_W-1)^2, \tag{51}$$

where ω_P and ω_W are the concentration of product and waste, respectively.

The results to be presented here are for $\lambda_a = 1$; other results produced for different values of λ_a at fixed q indicate that the separation factor is a very weak function of the sidewall temperature. The results for the separation factor are, however, strong functions of q, which indicates a strong dependence on the overall vertical temperature difference, ΔT. In this paper the unit of separative power is kg U/yr in contrast to that of Conlisk (1983, 1986*b*) in which the separative power units are in kg UF_6/yr. In this regard, for a true comparison with the other work in this area, the number 47.25 in table 3 of Conlisk (1986*a*) and table 2 of Conlisk (1986*b*) should read 32, i.e. 47.25 kg UF_6/yr = 32 kg U/yr.

On figure 6 are the results corresponding to $\dot{m}_F = 3\times10^{-4}$ kg/s for various values

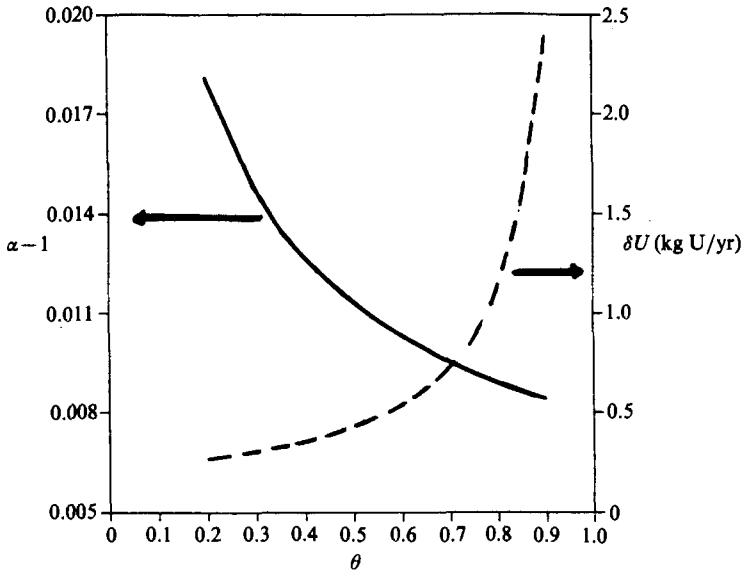

FIGURE 6. Separation factor and separative power as a function of cut for $a = 0.5$, $q = -3$, $\dot{m}_F = 3 \times 10^{-4}$ kg/s, $M = 3$, and $Z_0 = 10$.

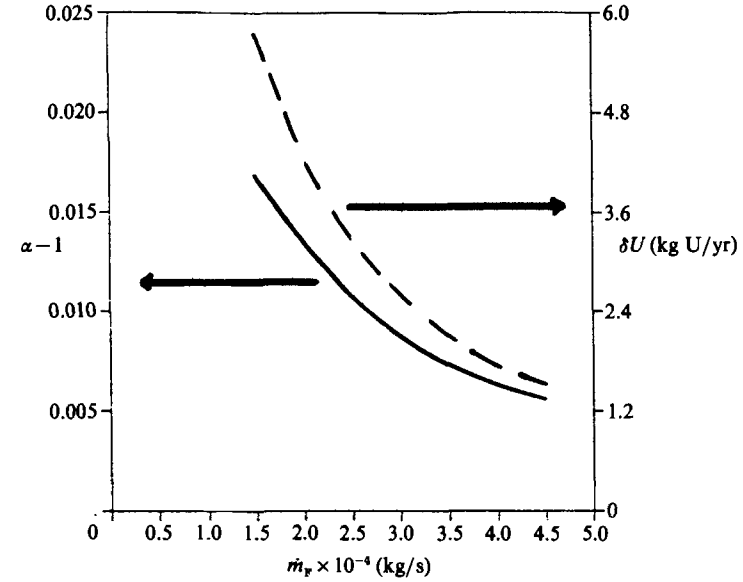

FIGURE 7. Separation factor and separative power as a function of feed flow rate $\dot{m}_F$; other parameters are as on figure 6.

of the cut at a Mach number $M = 3$; for $L/B_1 = 10$, as are the solutions shown here ($B_1 = 0.25$ m), this corresponds to an Ekman number $E = 1.061 \times 10^{-7}$ with $\delta = 0.05798$. The corresponding value of q is also given. On figure 7 are the results as a function of feed flow rate for fixed cut, $\theta = 0.5$. Note the rapid decrease in separative power as the feed flow rate increases, which is consistent with the results of Conlisk (1986*b*). Here $\alpha = \omega_P/\omega_F$ as in Conlisk (1986*b*).

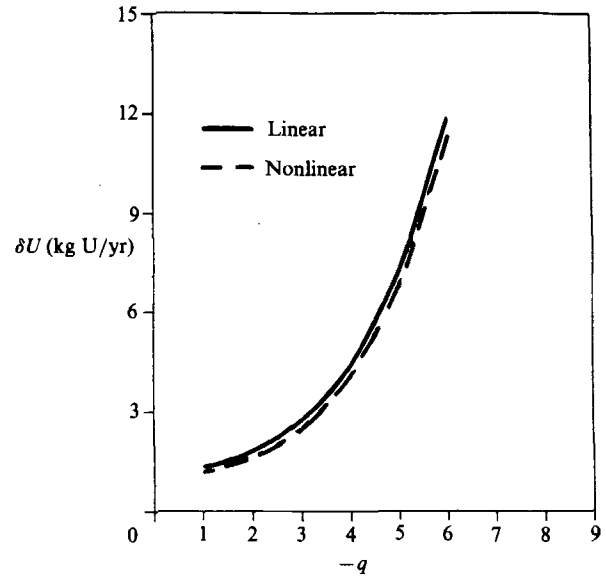

FIGURE 8. Separative power as a function of q for $a = 0.8$, $\theta = 0.5$ at $\dot{m}_F = 3 \times 10^{-4}$ kg/s, $M = 3$ as compared with the linear theory of Conlisk *et al.* (1983).

On figure 8 are results as a function of thermal drive parameter q for $\dot{m}_F = 10^{-4}$ kg/s. For $q \leqslant -6$ in figure 8, the mixture is not enriched and the separative power is meaningless; a similar comment applies to other cases. Note for these cases the rapid rise in separative power; in figure 8 it occurs for $q \sim -6$ and corresponds to $F_{\frac{1}{3}} \to 0$ in boundary condition (43). It should be noted that the solid line in the figure corresponds to the case where the $E^{\frac{1}{4}}$ layer is linear as considered in Conlisk *et al.* (1983). For this value of $\dot{m}_F$ there is little difference between the present results and those of Conlisk *et al.* (1983). Figure 9 shows a further comparison of the linear and nonlinear results as a function of flow rate. Note that even at a flow rate of 4.5×10^{-4} kg/s, the separation factor is still close to the linear result. There is a bit more error in the separative power results because of the multiplication by extremely large numbers; nevertheless the comparison is striking. The conclusion that must be reached here is that the regime $\delta = O(E^{\frac{1}{4}})$ is a very weak limit in terms of the mass transfer problem and the analytical closed-form solution for the separation factor given in Conlisk (1983) and Conlisk *et al.* (1983) may be employed with confidence far outside its technical range of validity.

The reason for this appears to be connected with the fact that the integral over z of the vertical flux in the $E^{\frac{1}{3}}$ layer is the same as the integral of the flux in the two shear layers in the linear problem. To see this note that (Conlisk *et al.* 1983)

$$\rho_e F_{\frac{1}{3}} = 1 - (1-\theta)\frac{z}{Z_0} + \frac{a\rho_e^{\frac{1}{2}} q}{2\sigma^{\frac{3}{4}}}\left\{\lambda_a\left(1 - 2\frac{z}{Z_0}\right) + \frac{z}{Z_0}\right\}$$

and consequently $$\int_0^{Z_0} \rho_e F_{\frac{1}{3}}\,\mathrm{d}z = Z_0\left(\frac{1+\theta}{2} + \frac{a\rho_e^{\frac{1}{2}} q}{4\sigma^{\frac{3}{4}}}\right) = \int_0^{Z_0} \rho_e F_s\,\mathrm{d}z$$

from (3.44) of Conlisk *et al.* (1983). (Note that the integral of the $E^{\frac{1}{4}}$-layer vertical flux over z is zero). This result suggests that the separation factor for the present nonlinear regime, which is based on a vertical integral of $1/(\rho_e F_{\frac{1}{3}})$ will be close to the

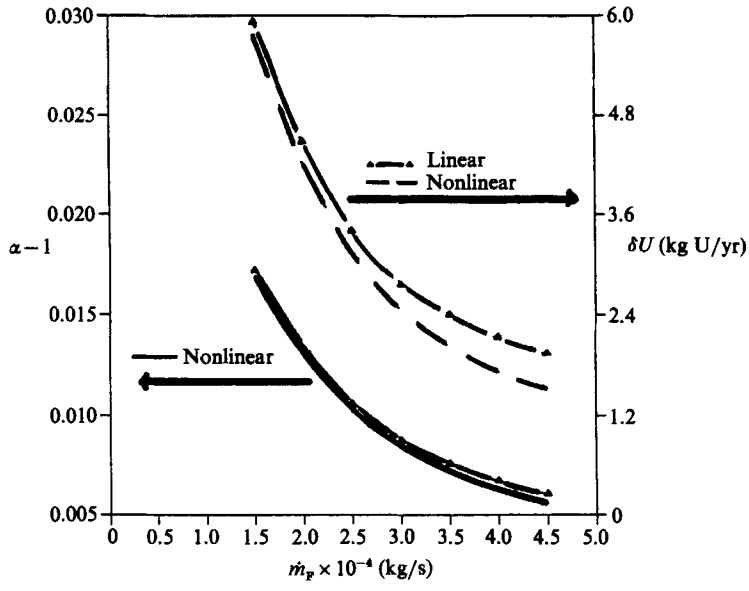

FIGURE 9. Comparison of the linear theory with the nonlinear theory for the separation factor and separative power; the linear results are taken from Conlisk *et al.* (1983). Here $M = 3$, $\theta = 0.9$, $a = 0.5$, $q = -3$.

result for the linear problem ($\partial\tilde{\omega}_1/\partial\xi$ in (43) is small based on the numerical results). This fact implies that the striking change in the $E^{\frac{1}{4}}$-layer flow patterns as λ is increased (figures 2 and 3) will have little effect on the separation factor (w_0 is still antisymmetric with respect to $z = \frac{1}{2}$) and implies that the vertical flow rate in the $E^{\frac{1}{3}}$ layer is the dominant influence on separation.

5. Summary and conclusions

In this paper solutions to the mass transfer problem for a binary gas mixture in a rapidly rotating centrifuge have been obtained in the parameter range for which the $E^{\frac{1}{4}}$ Stewartson layer is nonlinear. This corresponds to feed flow rates of about 1×10^{-4} to 1×10^{-3} kg/s based on typical parameters. The nonlinear compressible Ekman condition has been shown to be the same as that of Bennetts & Hocking (1973) provided that the parameter $h \ll 1$ and the Prandtl number $Pr \approx 1$. This condition has been employed to compute the flow patterns within the $E^{\frac{1}{4}}$ layers which are inputs to the solution for the concentration layers that form on the vertical sidewalls; particular interest has been focused on the source layer on $r = a$. It should be noted that the concentration-layer thickness is of the same width ($O(E^{\frac{1}{4}})$) as the outer Stewartson layer, in contrast to the parameter range discussed in Conlisk *et al.* (1983) and in Conlisk (1986*b*). In this regard it should be noted that the present results do not deviate substantially from previous work encompassing the range $E^{\frac{1}{4}} \ll \delta \ll E^{-\frac{1}{4}}$. Here $\delta = O(E^{\frac{1}{4}})$ and the qualitative trends concerning the dependence of the separation factor and the separative power on cut, feed flow rate, thermal drive parameter q, and other parameters are reproduced. Quantitatively the results are also not much different from the previous results and this fact is important in two ways. First, the present results suggest that the analytical, closed-form solution for the separation factor (and hence separative power) may be applied with confidence

far outside the technical range of validity of the formula. Second, the correct interpretation of this fact is that the $E^{\frac{1}{8}}$-layer flow patterns are the crucial factor in designing a centrifuge for maximum separative power.

As a practical matter, the present work indicates that the closed-form analytical solution for the separation factor given by Conlisk *et al.* (1983) gives accurate results from feed flow rates of about 1×10^{-5} to 1×10^{-3} kg/s and, consequently, complicated numerical solutions for the separation factor are not necessary for accurate design calculations.

The authors are grateful to Professor Michael R. Foster for his helpful comments and to Professor David Walker who originally derived equation (A 2).

Appendix A

The differential equation satisfied by the leading-order geostrophic temperature distribution, say $T_0(r, z)$ may be derived as follows. In the core region, from (2)

$$V_G = \tfrac{1}{2} r T_G + P(r), \tag{A 1}$$

where $P(r) = (1/2M)(\partial p/\partial r)$. We now use (3) to solve for u and substitute into (5). Finally V_G in that equation may be eliminated using (A 1) and the result is

$$\nabla^2(\sigma T_G) - \frac{2}{r}((\sigma-1)\,T_G) = -2hr\left\{\nabla^2 - \frac{1}{r^2}\right\}P(r) + \epsilon_f E^{-\frac{1}{2}}\rho_e(r)\,(Pr-1+\sigma)\,W_G\frac{\partial T_G}{\partial z}. \tag{A 2}$$

Note that for $\epsilon_f = O(E^{\frac{1}{4}})$, (A 2) describes a singular perturbation problem for T_G in which the core temperature distribution is adjusted to its sidewall value in a layer of width $O(E^{\frac{1}{8}})$. Thus, if we write $T = \lambda_a \lambda_T + T_G$ in this layer, then $T_G \to 0$ as $(r-a)E^{-\frac{1}{8}} \to 0$, i.e., as $\xi = (r-a)E^{-\frac{1}{4}} \to \infty$ since $E^{\frac{1}{4}} \ll E^{\frac{1}{8}}$. Consequently $\lim_{\xi\to\infty} \hat{T}_0 = 0$ to match the geostrophic distribution. The detailed core-temperature problem is complicated and the solution is tedious and will not be given here.

Appendix B

Here the details of the discretization are described for the numerical method to solve the nonlinear $E^{\frac{1}{4}}$-layer equations (28) and (30) subject to the conditions (29) and (31). The equation (28) can be written as

$$\frac{\mathrm{d}^2\phi}{\mathrm{d}\xi^2} + \lambda\kappa\phi\frac{\mathrm{d}\phi}{\mathrm{d}\xi} + 2\kappa\phi = 0, \tag{B 1}$$

where κ is a constant.

For the mesh size $\Delta\xi = h_0$ standard central-difference approximations were used for each of the derivatives in (28) and (30) and these are written according to

$$\left.\frac{\mathrm{d}\phi}{\mathrm{d}\xi}\right|_{\xi j} = \frac{1}{2h_0}(\phi_{j+1} - \phi_{j-1}), \tag{B 2}$$

$$\left.\frac{\mathrm{d}^2\phi}{\mathrm{d}\xi^2}\right|_{\xi j} = \frac{1}{h_0^2}(\phi_{j+1} - 2\phi_j + \phi_{j-1}). \tag{B 3}$$

For (28) the finite-difference equations are thus given by

$$\phi^i_{j+1}(1 + \lambda\kappa h_0\,\phi^{i-1}_j) + \phi^i_j(2\kappa h_0^2 - 2) + \phi^i_{j-1}(1 - \tfrac{1}{2}\kappa\lambda h_0\,\phi^{i-1}_j) = 0. \tag{B 4}$$

Here j denotes a typical location in the mesh and $0 \leqslant j \leqslant N$, where N is the total number of mesh points, and i is the iteration number.

This equation defines a tri-diagonal system of equations which were solved using the Thomas algorithm. The iteration scheme is assumed to converge when

$$\frac{\phi_j^i - \phi_j^{i-1}}{\phi_j^i} < \epsilon_1,$$

where $\epsilon_1 = 1 \times 10^{-4}$–$1 \times 10^{-5}$. In this study the maximum number of iterations required was less than 20. Equation (30) was solved using the same method and the results for the velocity field were input into the mass transfer problem. Note that the flow velocities in the $E^{\frac{1}{4}}$ layer do not depend explicitly on temperature in the present problem.

REFERENCES

BARCILON, V. 1970 Some inertial modifications of the linear viscous theory of steady rotating fluid flows. *Phys. Fluids* **13**, 537–544.

BENNETTS, D. A. & HOCKING, L. M. 1973 On nonlinear Ekman and Stewartson layers in a rotating fluid. *Proc. R. Soc. Lond.* A **333**, 469–489.

BIRD, R. B., STEWART, W. E. & LIGHTFOOT, E. N. 1960 *Transport Phenomena*. Wiley.

CONLISK, A. T. 1983 The effect of source–sink geometry on enrichment in a gas centrifuge. *Phys. Fluids* **26**, 2946–2957.

CONLISK, A. T. 1986*a* Fluid dynamics and design of gas centrifuges. In *Encyclopedia of Fluid Mechanics* (ed. N. Cheremisinoff), vol. 2, ch. 46. Gulf.

CONLISK, A. T. 1986*b* The effect of aspect ratio and feed flow rate on separative power in a gas centrifuge. *Chem. Engng Sci.* **41**, 2639–2650.

CONLISK, A. T., FOSTER, M. R. & WALKER, J. D. A. 1983 Fluid dynamics and mass transfer in a gas centrifuge. *J. Fluid Mech.* **125**, 283–317.

CONLISK, A. T. & WALKER, J. D. A. 1982 Forced convection in a rotating annulus. *J. Fluid Mech.* **122**, 91–108.

HIDE, R. 1968 On source–sink flows in a rotating fluid. *J. Fluid Mech.* **32**, 737–764.

KAI, T. 1975 Basic characteristics of centrifuges. I. Analysis of concentration distribution in centrifuge. *J. Atmos. Environ. Soc. Japan* **17**, 131–140.

KAI, T. 1977 Basic characteristics of centrifuges. II. Analysis of fluid flow in centrifuges. *J. Nucl. Sci. Tech.* **14**, 267–281.

OLANDER, D. R. 1981 The theory of uranium enrichment by the gas centrifuge. *Prog. Nucl. Energy* **8**, 1–33.

SOUBBARAMAYER 1979 Centrifugation. In *Uranium Enrichment* (ed. S. Villani), pp. 183–244. Springer.

WOOD, H. G. & SANDERS, G. 1983 Rotating compressible flows with internal sources and sinks. *J. Fluid Mech.* **127**, 299–313.